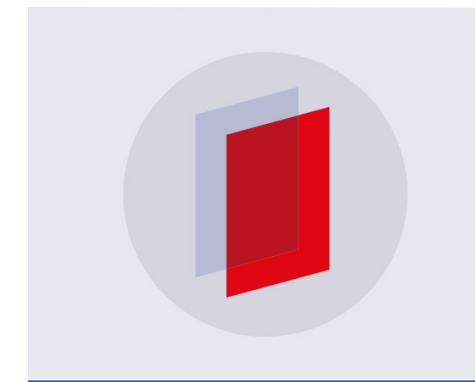
PAPER

Pattern formation in strongly magnetized plasmas: observations from the magnetized dusty plasma experiment (MDPX) device

To cite this article: E Thomas Jr et al 2020 Plasma Phys. Control. Fusion 62 014006

View the article online for updates and enhancements.



IOP ebooks™

Bringing you innovative digital publishing with leading voices to create your essential collection of books in STEM research

Start exploring the collection - download the first chapter of every title for free.

Plasma Phys. Control. Fusion 62 (2020) 014006 (11pp)

https://doi.org/10.1088/1361-6587/ab410c

Pattern formation in strongly magnetized plasmas: observations from the magnetized dusty plasma experiment (MDPX) device

E Thomas $Jr^{1,4}$, B Lynch 1 , U Konopka 1 , M Menati 1 , S Williams 1 , R L Merlino 2 and M Rosenberg 3

E-mail: etjr@auburn.edu

Received 10 July 2019, revised 14 August 2019 Accepted for publication 3 September 2019 Published 18 October 2019



Abstract

The last decade has seen the development of new experimental devices to explore the physics of magnetized dusty plasmas. Because of the small charge-to-mass ratio of the charged microparticles, it is necessary to operate these experiments at high magnetic fields of several Tesla in order to observe the direct effect of the magnetic forces on the transport properties of the charged microparticles. While the study of magnetized dusty plasmas is still the ultimate goal, these experiments have also provided new opportunities to studies regimes of strongly magnetized, low temperature, laboratory plasmas that have not been extensively explored. Experiments show the formation of new types of self- and imposed-ordered structures that form in both the plasma and among the microparticles. This paper summarizes recent experimental observations of plasma filamentation (in the plasma) and will discuss possible connections to 'dust gridding' phenomena that are observed in the magnetized dusty plasma experiment device.

Keywords: dusty plasma, magnetic fields, filamentation, superconducting magnet, pattern formation

(Some figures may appear in colour only in the online journal)

1. Introduction

Dusty plasma research has made significant advances over the last three decades. In these plasmas, the electrons, ions, and neutral atoms that form a typical plasma are joined by a fourth component—solid, charged, particulate matter (i.e. 'dust grains'). These dust grains, which range in size from a few nanometers to several micrometers, collect charge from the background plasma and become incorporated as an additional plasma species [1, 2] Although these particles can become highly charged with hundreds to thousands of elementary charges, their large mass relative to the electrons and ions means that the charge-to-mass ratio of the dust particles can be quite low. This has profound consequences for the operation of dusty plasma experiments as well as the physical properties of these systems.

The most immediate consequence of the low charge-tomass ratio is the fact that the dynamics of the dust component of the plasma is dramatically slowed compared to the dynamics of the electrons and ions. Consider a typical laboratory dusty plasma with electron/ion densities, $n \sim 10^{15} \, \mathrm{m}^{-3}$, electron temperature, $T_e \sim 2.5 \, \text{eV}$, ion temperature, $T_i \sim 1/40 \, \text{eV}$, and 1-micron diameter dust particles with a mass, $m_d \sim 10^{-15}$ kg, carrying $Z_d \sim 1000$ elementary charges, and dust number density, $n_d \sim 10^9 \, \mathrm{m}^{-3}$. The electron (ω_{pe}) and ion (ω_{pi}) plasma frequencies, (where $\omega_{ps} = \left[\frac{n_s q_s^2}{\epsilon_0 m_s}\right]^{1/2}$, n_s , q_s , and m_s are the density charge and

density, charge, and mass of plasma species, s = electron(e),

¹ Physics Department, Auburn University, Auburn, AL, United States of America

² Department of Physics and Astronomy, University of Iowa, Iowa City, IA, United States of America

³ Department of Electrical and Computer Engineering, University of California—San Diego, La Jolla, CA, United States of America

⁴ Authors to whom any correspondence should be addressed.

ion(*i*) or dust (*d*)) are $1.8 \times 10^9 \,\mathrm{rad} \,\mathrm{s}^{-1}$ and $6.6 \times 10^6 \,\mathrm{rad} \,\mathrm{s}^{-1}$, respectively. By contrast, the dust plasma frequency is $54 \,\mathrm{rad} \,\mathrm{s}^{-1}$. This means that fundamental processes of the dust component have become slowed to the point where they can be directly visualized in the plasma using tools as simple as high-speed cameras. This enables studies of the collective behavior of the dust component, e.g. shocks [3–6], vortices [7–9], and waves [10–13], with unprecedented precision, due to of the ability to study plasma dynamics at an 'atomistic' level.

In addition to this slowing of the dust component

dynamics, the large charge on the dust particles also contributes to the ability of a dusty plasma to form ordered patterns. This is because it becomes possible to tune the dynamics of a dusty plasma through the Coulomb coupling parameter, the ratio of the electrostatic potential energy to thermal energy, $\Gamma = \frac{q_d^2}{4\pi\varepsilon_0\Delta k_BT_d}$; where, Δ is the average spacing between the particles, k_B is Boltzmann's constant, and T_d is the kinetic temperature of the dust component. Numerous studies over the past three decades have shown that laboratory dusty plasmas experiments can be performed from the weakly-coupled ($\Gamma \ll 1$) to strong-coupled ($\Gamma \gg 1$) regimes. In particular, the self-organization of the dust component of the plasma that arises in the strongly-coupled regime is not only a scientifically interesting physical system that can be studied on its own, it also provides a well-defined initial state from which to perform a variety of other plasma experiments [14-18].

The studies described above can all be considered to be electrostatic experiments. That is, the dust particles are introduced into a laboratory plasma, they become charged, and they remain suspended in the plasma due to a zero-order equilibrium that is established between the gravitational force and a compensating electric force in the plasma sheath. In recent years, interest has grown in studying the influence of magnetic fields on dusty plasmas [19-27], but this is where a second consequence of the low charge-to-mass ratio plays a role. In order for the dynamics of the dust component of the plasma to be influenced by a magnetic field, it can be shown, that magnetic fields, $B \ge 1$ T are required [28]. The application of these high magnetic fields to dusty plasma experiments has led to the discovery of new types of pattern formation and self- and imposed-ordering processes in both the background plasma and the dust particles.

This paper will report on experiments that have been performed on the magnetized dusty plasma experiment (MDPX) device at Auburn University. It will primarily focus on an analysis of plasma filaments, structures that form in the plasma along the magnetic field lines. It will be shown that the spatial properties of the filaments vary with neutral pressure and applied radio-frequency (rf) power and may be dependent on the ion magnetization. The paper will then discuss possible connections between the filaments and the imposed dust gridding phenomenon that were discovered in the MDPX device and that have been reported in previous papers [29–31]. Finally, this paper will briefly describe results

from recent simulation efforts that are being performed to understand the properties of the filaments.

This paper is organized in the following manner. Section 2 will discuss the setup of the MDPX device. Section 3 will focus on an analysis of plasma filaments that have been formed several different experiments on the MDPX device. Section 4 will give a brief discussion on the dust gridding phenomenon and its similarity with the filament. Finally, section 5 will discuss some of the simulation efforts and then provide a summary of the work that is described in this paper.

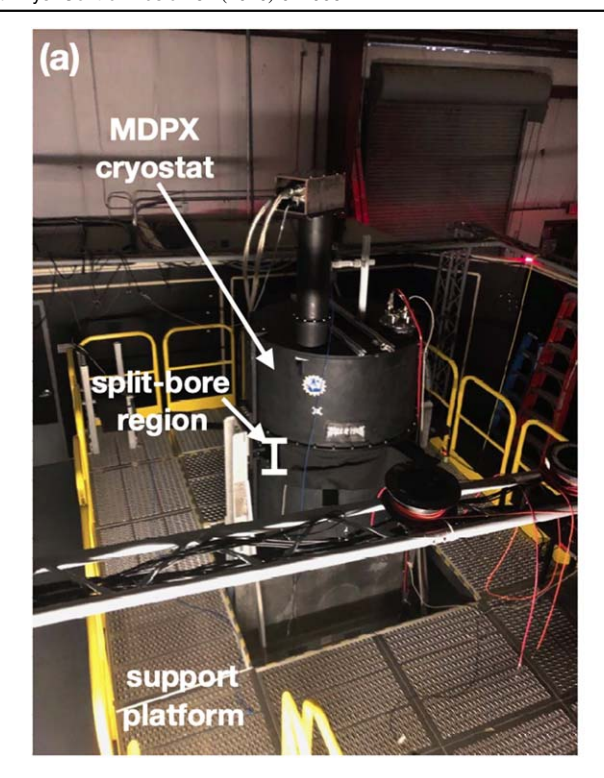
2. The MDPX device

The MDPX device is a multi-configuration, multi-user research experiment that is designed to study the dusty plasmas that extend from the regime of strongly magnetized plasmas (where the electrons and ions are magnetized but the charged dust is unmagnetized), to the regime of magnetized dusty plasmas (where the dynamics of the electrons, ions, and charged dust particles is dominated by magnetic forces). The design, construction, and initial operation of the MDPX device have been described in detail in previous papers [32–34], so only a brief overview of the experiment is given here.

The MDPX device consists of two integrated components: a superconducting magnet system and a plasma source. A photograph showing an overview of the laboratory facility is shown in figure 1(a). A key feature of the MDPX design is that the plasma source can be easily removed from the magnet, so that a number of different plasma source configurations can be used. All of the experiments described in this paper use the primary 'MDPX octagon' plasma source, so only this source will be discussed.

The superconducting magnet system consists of four cylindrical coils placed in a large, split-bore cryostat, the large black structure at the center of figure 1(a). The cryostat has an outer diameter of 127.8 cm with an inner, 50 cm diameter 'warm bore' that extends the full axial length, 93.5 cm, of the cryostat. The upper and lower halves of the cryostat are separated by four posts that create a 19 cm axial gap. This open, split-bore design allows both radial and axial access to a large central region where the strongest magnetic fields are formed. Although the experiments reported here are performed using a uniform magnetic field configuration, the electrical control system for the magnet allows individual currents to be applied to each coil allowing magnetic field configurations ranging from linear gradients to cusp-like geometries to be formed. The magnet system is designed to produced uniform magnetic fields up to B = 4 Tesla and axial gradients up to $1 \,\mathrm{T}\,\mathrm{m}^{-1}$.

The experiments reported in this paper were all performed in the MDPX octagon plasma chamber. This is a custom-designed aluminum vacuum chamber with a cylindrical interior that is 36.6 cm in diameter and 17.8 cm in height. The exterior of the vacuum chamber has eight flat faces which use rectangular flanges for probe or viewports—giving the



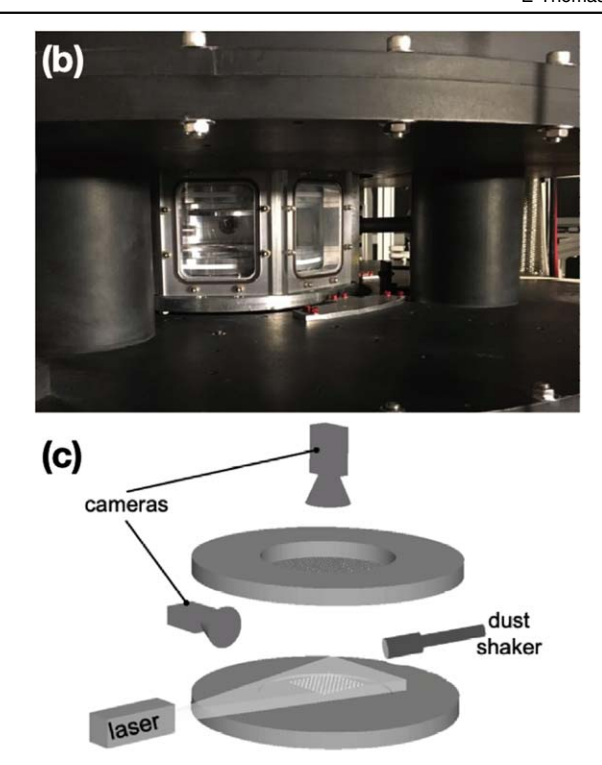


Figure 1. (a) Overview photograph of the Magnet Laboratory that houses the magnetized dusty plasma experiment (MDPX) device. The main cryostat with the split 'warm bore' is identified in the photograph. An aluminum support platform and cable/fiber optic trays are also visible in the image. (b) A close-up photograph of the MDPX octagon plasma source mounted inside the split 'warm bore' of the magnet. Two of the octagon faces of the plasma chamber are visible as are two of the four support posts that separate the upper and lower sections of the cryostat. (c) A schematic drawing of the interior setup of the electrodes, camera, and dust shaker.

chamber its octagonal shape. The flanges have fittings that adapt to standard ISO or conflat vacuum components in order to maximize the flexibility of the design allow relatively easy installation of plasma diagnostics. A photograph showing a closeup view of the MDPX octagon plasma chamber mounted in the inner bore of the magnet system is shown in figure 1(b). This design maximizes both optical and probe access to the plasma volume and is unique among the various high magnetic field dusty plasma experiments.

A schematic drawing of the interior of the plasma chamber is shown in figure 1(c). Capacitively-coupled, rf glow discharge plasmas are generated between a pair of parallel plate electrodes that can be separated between 6.0 and 9.0 cm. The applied rf power is at a fixed frequency of 13.56 MHz and is typically delivered at a power level between 1 and 10 W for most of the experiments. Both electrodes are aluminum plates that are 30.5 cm in diameter. The lower electrode has a 15.2 cm diameter, 0.64 cm circular depression at its center which helps to provide radial confinement of dust particles. The upper electrode has a 10.2 cm diameter through-hole to provide optical access to the plasma volume from the top. Depending upon the experimental configuration, this hole is usually covered with a conducting material to prevent a significant perturbation of the main plasma volume. Either a conducting glass plate, i.e. FTO (fluorine-doped tin-oxide)-coated glass or a high-transparency woven wire mesh is used.

All of the experiments that will be discussed in this paper will be performed using a powered lower electrode and with the upper electrode electrically floating. In practice, whether the upper electrode was powered for floating does not significantly alter whether the filaments, dust grids, or other types of patterns form, but could modify the threshold conditions for the formation or the precise details of the patterns. Similarly, it is also noted that the spacing between the electrodes may also impact the threshold conditions for various types of pattern formation. For most of the experiments reported here, a magnetic field, $B \ge 0.5$ T, is needed in order to observe the phenomena reported in this paper.

3. Observations of plasma filamentation

The primary focus of this paper will be an analysis of the plasma filamentation phenomenon at high magnetic field. For this work, we define the filaments as elongated structures that form along magnetic field lines between the two electrodes of a capacitively-coupled rf discharge. In the MDPX device, we can observe filaments via side views or top views as shown in figure 2 that are visibly similar to phenomena reported in earlier works [23, 35–37]. The filaments can appear in the experiment as quasi-stationary isolated cylindrical structures (a vertical column when viewed from the side or a dot when viewed from above) or as continuous collective structures such as spirals or rings that slowly evolve in time over tens of

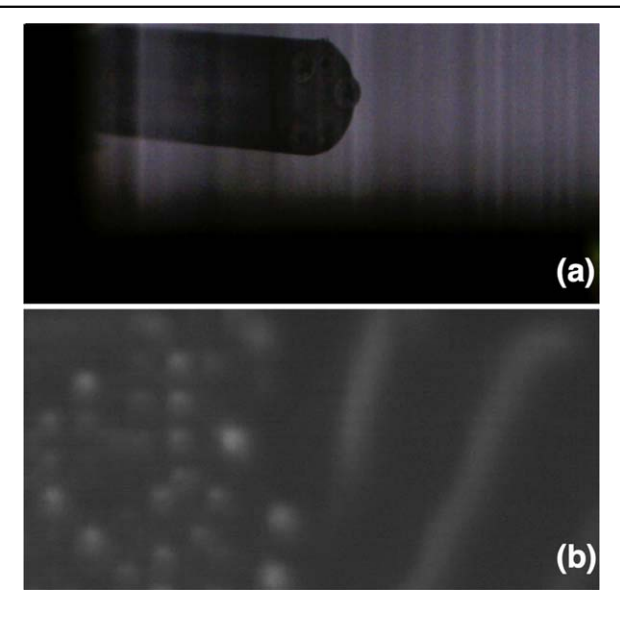


Figure 2. Cropped (a) side and (b) top view of filaments in an argon plasma at B=0.75 T, P=2.9 Pa, and rf power =1.8 W. Vertically aligned filaments are shown throughout the plasma volume. The large object in the center of the image is the dust shaker. In (b), we see two types of filamentary structures—individual filament 'columns', which appear to the left as dots, and longer extended structures, which appear to the right as lines. It is noted that, in this case, these structures are not stationary, they are continuously moving.

seconds. For most of the analysis that is considered here, views from the top camera will be used.

For the first two experimental results, the formation of the filaments is examined as a function of neutral pressure, as shown in figure 3, and as a function of rf power, as shown in figure 4. The experiment is performed in the MDPX octagon chamber with a conducting FTO glass plate on the top electrode. The separation between the two electrodes in the plasma source is 6.2 cm. Argon plasmas are made at rf powers between 0.8 and 5.0 W and at neutral pressures ranging from 2 to 9 Pa. In both figures, the filaments are viewed from the top using a 4 MPixel video camera that is operating at 12.5 frames per second and with a spatial resolution of 0.07 mm/pixel (70μ m/pixel).

In figure 3, the development of the filaments is shown as a function of neutral pressure from lower pressure in 3(a) at $P=2.9\,\mathrm{Pa}$ to a higher pressure in 3(g) at $P=8.4\,\mathrm{Pa}$. The experiment is performed in argon gas at a constant applied rf power of 1.8 W and at a constant magnetic field $B=0.75\,\mathrm{T}$. If it is assumed that the ions are room temperature ($T_i=1/40\,\mathrm{eV}$), they will have a thermal velocity given by $v_{th}=\sqrt{\frac{8kT_i}{\pi m_i}}=$ $\sim 390\,\mathrm{m\,s^{-1}}$, which will correspond to an ion gyroradius, $\rho_i=0.22\,\mathrm{mm}$. This scale size is compared with the ion-neutral mean free path, which is computed from $\lambda_{mfp}=\frac{1}{N_0\sigma_{in}}$, where N_0 is the number density of the neutrals and σ_{in} is the ion-neutral collision cross-section which is calculated to be $3.27\times10^{-18}\,\mathrm{m}^{-2}$ based upon a method described by Khrapak [38]. For the pressure ranges in this experiment, the ion-neutral mean free path will range from $\lambda_{mfp}=0.42\,\mathrm{mm}$ (approximately twice the

ion gyroradius) at $P = 2.9 \,\text{Pa}$ in figure 3(a) to $\lambda_{mfp} = 0.14 \,\text{mm}$ (approximately one-half the ion gyroradius) at $P = 8.4 \,\text{Pa}$ in figure 3(g).

It is observed that the filaments appear as individual structures, e.g. dots in figures 3(a) and (b), that appear to merge into each other with increasing pressure, forming ring-like structures as seen in figures 3(c) and (d). As the pressure continues to increase, the ring-structures begin to fade and the appearance of the plasma becomes more uniform. In the experiment, as the pressure continues to rise above 10–13 Pa, the ring structures completely dissipate, and the plasma becomes uniform in appearance.

The properties of these filaments may also be considered in terms of the degree of magnetization of the ions. This magnetization can be calculated from the dimensionless Hall parameter, which is given as the ratio of the cyclotron frequency $(\Omega_{cs} = q_s B/m_s)$ to the neutral collision frequency $(f_{ns} = N\sigma v_{ts})$; i.e. $H = \frac{\Omega_{cs}}{f_{ns}}$. The variables q_s , m_s , and v_{ts} are the charge, mass, and thermal velocity of the species, s = electrons(e), ions (i), or dust (d), respectively, and f_{ns} is the collision frequency between the neutral atoms and species, s. Because of the discrepancy between the cyclotron frequency (which is given in terms of an angular velocity) and the collision frequency (which is given in terms of a real frequency), a modified Hall parameter, $H_{\text{mod}} = (H/2\pi)$ will be computed. H_{mod} is mathematically equivalent to the ratio of the mean free path $\lambda_{mfp} = 1/N\sigma$ divided by the circumference of a gyro-orbit $(2\pi\rho_s)$. Therefore, the modified Hall parameter can be physically interpreted as the number of complete gyro-orbits that can be made by a charged particle in a magnetic field prior to making a collision, $H_{\mathrm{mod}} = \frac{\lambda_{\mathrm{mfp}}}{2\pi\rho_{\mathrm{s}}}$.

In the case of the filaments considered here, with increasing pressure, the modified Hall parameter will be decreasing from $H_{\rm mod}=0.3$ at 2.9. Pa to $H_{\rm mod}=0.1$ at 8.4 Pa. This may be interpreted that, as a function of the neutral pressure, the appearance of the filaments is being suppressed by the ion-neutral collisions. One feature to note in figure 3 is the appearance of the filament free region at the center of the system with increasing pressure. It remains to be determined why this region did not continue to form additional filaments; this will be the subject of future experiments.

In figure 4, the development of the filaments is shown as a function of rf power from a lower power of 0.87 W in figure 4(a) to a higher power of 4.7 W in figure 4(g). The experiment is also performed in argon gas but at a constant neutral pressure of 4.6 Pa and at a constant magnetic field B = 0.75 T. At B = 0 T, the plasma density for this configuration in this rf power range extends from $n \sim 0.4$ to 1.2×10^{15} m⁻³. Although this a factor of three increase in the plasma density, the ionization fraction in the plasma varies from ~ 3 to 9×10^{-7} .

Although we have attempted to perform more detailed measurement of the plasma parameters in the presence of the magnetic field, Langmuir probe measurements have proven to be unreliable for $B \geqslant 0.25$ T—particularly for the electron collection—in these experiments. Nonetheless, our previous measurements have indicated that the ion saturation current

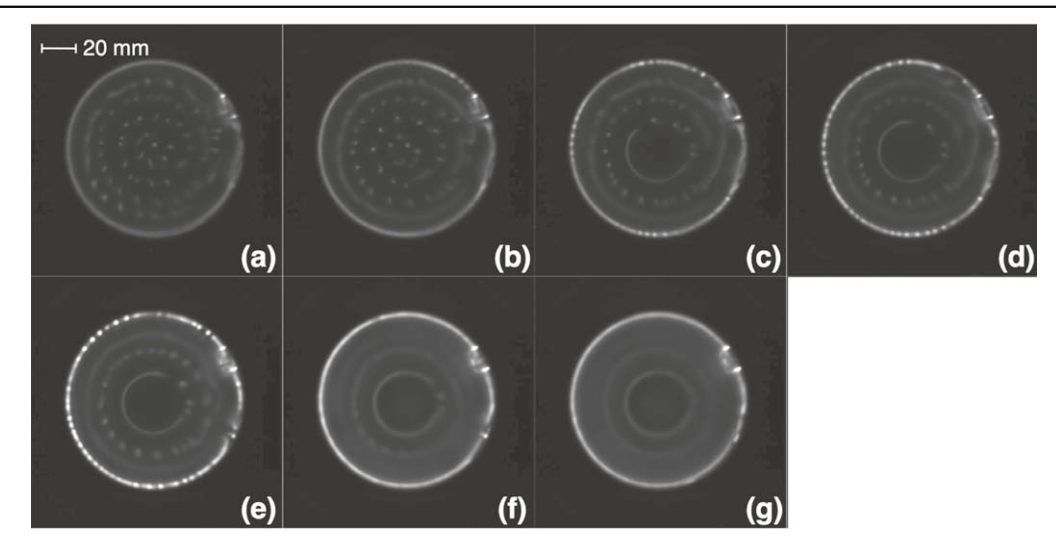


Figure 3. Top view of filaments in an argon plasma at B = 0.75 T, rf power = 1.8 W with the neutral pressure varying from: (a) 2.9 Pa, (b) 3.6 Pa, (c) 4.1 Pa, (d) 4.6 Pa, (e) 5.7 Pa, (f) 6.8 Pa, (g) 8.4 Pa. With increasing pressure, the filaments evolve into ring-like structures that, at even higher pressures, eventually fade and the plasma becomes stable.

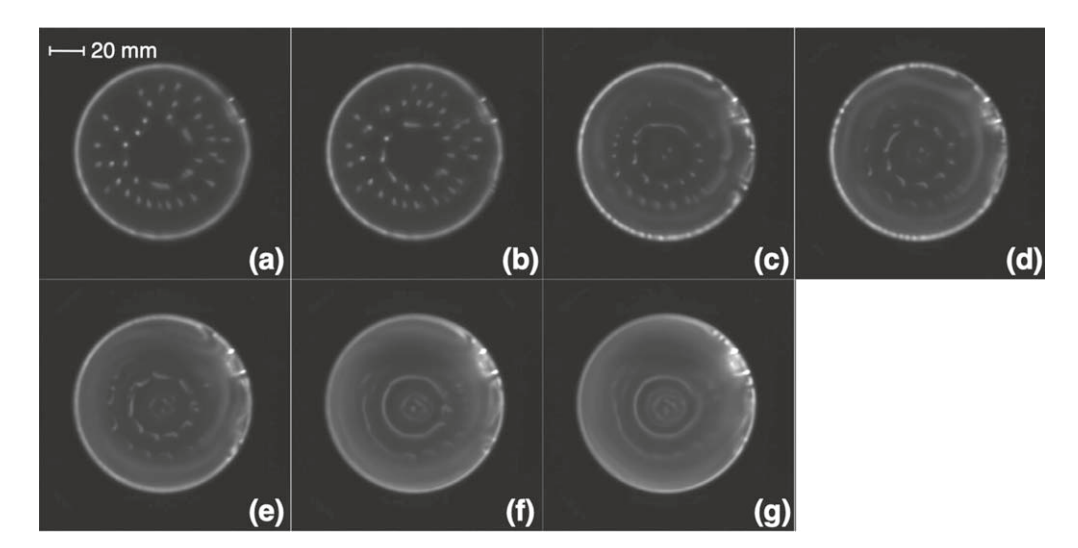


Figure 4. Top view of filaments in an argon plasma at B = 0.75 T, p = 4.6 Pa with the rf power varying from: (a) 0.87 W, (b) 0.98 W, (c) 2.0 W, (d) 2.3 W, (e) 2.8 W, (f) 3.7 W, (g) 4.7 W. With increasing rf power, the filaments evolve from individual dots to ring-like structures. However, at even higher applied power, the rings persist and appear to continue to evolve into other structures.

may vary by a factor of \sim 5 over the range from 0 to 2 T [39]. Therefore, we believe that dominating role of ion-neutral collisions will persist during the variation in the rf power.

Recently, a new study of filaments was performed in a new spatial configuration of the MDPX octagon chamber. The experiment was again performed in rf generated argon plasmas with a powered lower electrode and a grounded upper electrode with a conducting glass plate. For the results that are shown in figure 5, the electrode gap has been increased from 6.2 to 9.0 cm, the magnetic field is B = 1.0 T, and the neutral pressure is held fixed at P = 13.3 Pa. In this experiment, the rf power is ramped from 5(a) at 5 W to 5(g) at 40 W. The experiment is viewed from the top, but the camera is operating at a faster frame rate of 84 frames s⁻¹.

Even though the experimental configuration is different, the same qualitative features of the filaments observed in figure 4(g) at 4.7 W are also observed in figure 5(a) at 5.0 W. There are concentric rings of possibly merged filaments that surround a center that has a dense collection of individual filament 'spots'. As the rf power is increased, there is a dissipation of the rings. However, a new feature appears, a smaller scale 'spotty' structure that eventually extends over the entire field of view at the highest applied powers. It is noted that this transition from large- to small-scale structures has been tested under a variety of experimental conditions beyond those illustrated here and a small-scale structure appears with increasing RF power.

To characterize the properties of these structures, an analysis is performed, using the *ImageJ* application [41], of the light intensity of images over the central region of the filament structure as illustrated in figure 6. The analysis region is a rectangular box that is 820 pixels wide by

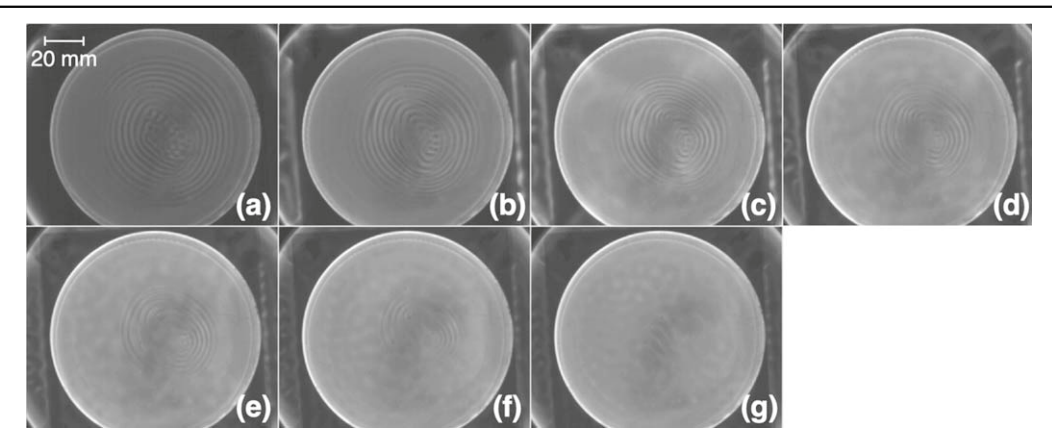


Figure 5. Top view of filaments in an argon plasma at B = 1.0 T, P = 13.3 Pa with the rf power varying from: (a) 5.0 W, (b) 10 W, (c) 15 W, (d) 20 W, (e) 25 W, (f) 30 W, (g) 40 W. Figure 5(a), 5(c), 5(e) and 5(g) are reprinted from [40], with the permission of AIP Publishing.

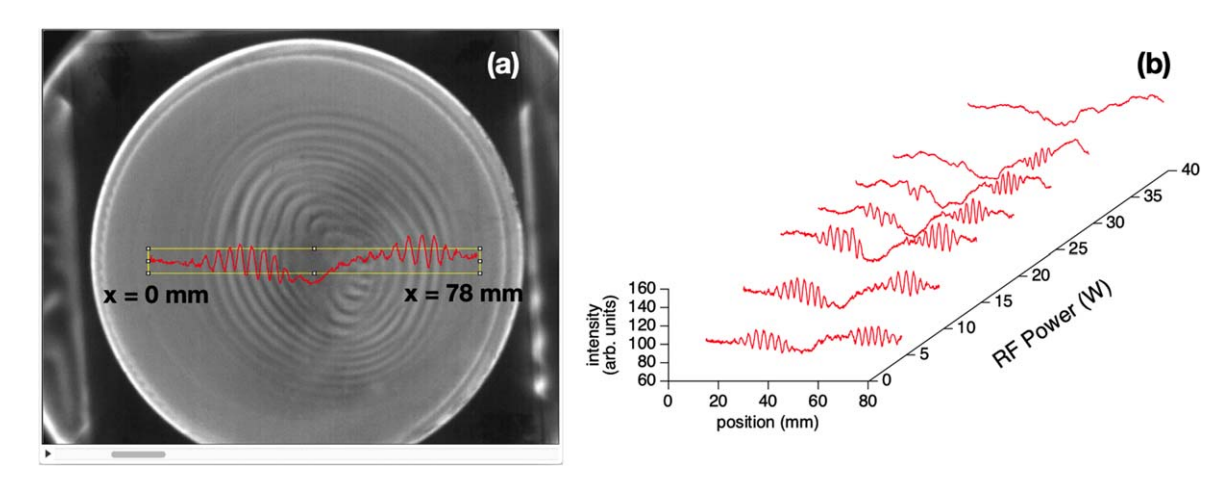


Figure 6. (a) Image of the analysis region (yellow box) that is used to characterize the spatial structure of the filament rings. The red curve is a measurement of the relative light intensity as a function of position with the analysis region. (b) Waterfall plot showing the evolution of the spatial structure of the filament in the analysis region as a function of increasing rf power.

60 pixels tall. The average light intensity is computed along each vertical column. In figure 6(a), the analysis region is shown for the rf power $= 10\,\mathrm{W}$ case. The red curve shows the fluctuation in the light intensity as a function of the horizontal position with peaks coincident with locations of the filament rings. In figure 6(b), a waterfall plot is shown that gives a qualitative comparison of the light intensity curves within the analysis box that correspond to the seven rf power settings displayed in figure 5. With increasing rf power, the larger fluctuations at the locations of the filament rings are shown to decrease in number and amplitude.

To extract more quantitative information about the light intensity fluctuations, a further analysis of these light intensity plots is presented in figure 7. Figures 7(a)–(c) show the spatial profiles of the light intensity over the length of the analysis box for the 5 W, 20 W, and 40 W cases, respectively. The plots clearly show the decay of the large filament rings. Figures 7(d)–(f) show the Fourier transforms of the average light intensity data for the 5 W, 20 W, and 40 W cases, respectively, and reveal several important features about the plasma. First, for the 5 W and 20 W cases, the Fourier transform shows the presence of a spatial mode with $1/\lambda_{\rm f}\sim 0.35~{\rm mm}^{-1}$ or $\lambda_{\rm f}\sim 3.0~{\rm mm}$. This

spatial mode corresponds to the presence of the filament rings that appear in figures 5(a)–(e) and the large amplitude, periodic structure in figures 7(a) and (b). More interesting is the appearance, first in figure 7(e) and more clearly in figure 7(f) of a coherent spatial mode with $1/\lambda_{\rm f}\sim 1.3~{\rm mm}^{-1}$ or $\lambda_{\rm f}\sim 0.8~{\rm mm}$. This is interpreted as a transformation of the filaments from large-scale spatial structures to smaller scale structures. Furthermore, it is noted that in the videos associated with these images at the higher powers there is a rapid fluctuation in the light intensity of the plasma—which may also be indicative of filamentary structures that are present, but beyond the detection limits of our current imaging systems.

4. Is dust gridding connected to filamentation?

The formation of the plasma filaments is not the only type of pattern formation process that is present in the MDPX device at high magnetic field. It was recently discovered that when high magnetic field experiments, at $B \geqslant 0.75\,\mathrm{T}$, were performed using a wire mesh embedded in the top electrode, the dust particles could take on spatial patterns that corresponded

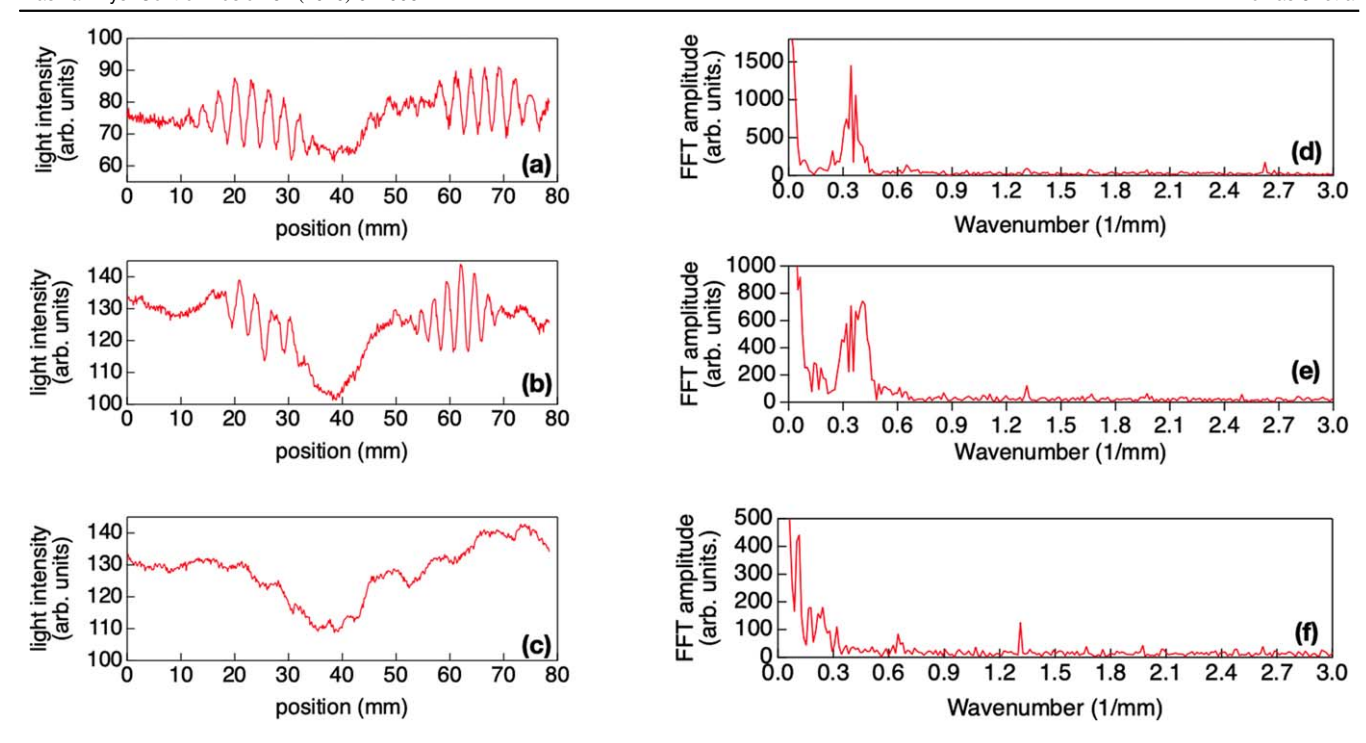


Figure 7. Spatial analysis of the light intensity information. Plots (a) rf power = 5 W, (b) rf power = 20 W, and (c) rf power = 40 W show the spatial profiles of the light intensity. Fourier transforms of these plots are shown in (d) 5 W data, (e) 20 W data and (f) 40 W data. For (d) and (e), the peak at wave number $1/\lambda \approx 0.35 \text{ mm}^{-1}$ corresponds to the large-scale spatial structure with $\lambda \sim 3.0 \pm 0.2 \text{ mm}$. For (e) and (f), there is the emergence of a peak at $1/\lambda \sim 1.3 \text{ mm}^{-1}$, which corresponds to the appearance of a small-scale structure $\lambda \sim 0.8 \text{ mm}$.

to the shape and spacing of the mesh [29, 30]. Past experiments have been performed to show that the dust gridding phenomenon scales with pressure: the particles become locked to the pattern of the mesh with lower pressures (i.e. at higher ion Hall parameter) and will become decoupled from the mesh with increasing pressure [31]. Additionally, recent simulations show that if the mesh acts to create a local perturbation in the plasma potential, the resulting potential wells can act to trap the dust particles and guide their motion in a manner that is qualitatively consistent with the experimental observations [42].

While the experimental observations of filaments reported in section 3 were performed when a conducting glass plate was placed on the upper electrode, filaments may also form when the wire mesh is used. In these experiment, rf generated argon plasmas are generated in the MDPX device at magnetic fields $B \geqslant 1.5$ T. These experiments were performed in the MDPX octagon plasma source using the same electrode gap, 6.2 cm, as was used in figures 3 and 4. The dust particles are 0.5-micron diameter silica microspheres.

This is illustrated in figure 8 which shows the combination of individual filaments (bright dots) with the dust grids. The images shown in figure 8 represent a sum of the maximum intensity from 50 individual video frames in order to reveal the pattern that has been imprinted onto the dust particles suspended in the plasma. Here, 0.5 micron diameter particles are suspended in argon plasmas beneath a #40 titanium wire mesh that had 0.25 mm diameter wires and a center-to-center spacing between wires of 0.635 mm. The two close-up regions show that the filaments are completely

surrounded by the ordered pattern of the dust particles. While the grid pattern is clearly disrupted by the filaments, the filaments appear to be relatively unaffected by the presence of the dust particles.

The coexistence of the dust gridding with the plasma filamentation leads to an obvious question: Are there connections between the two phenomena? To address this, two observations are considered. The first observation is the vertical extent of both the filaments and the dust grids. As shown in figure 2, under the right conditions, the plasma filaments can have a vertical extent that covers nearly the entire plasma volume, from the upper to the lower electrodes. This observation is quite intriguing because the ion-neutral collision mean free path for most of the experiments considered here is: $1 \text{ mm} \leqslant \lambda_{mfp} \leqslant 3 \text{ mm}$. The vertical extent of the filamentary structure to as much as 5-6 cm suggests that the electron (and ion) transport along the magnetic field lines dominates the transverse motion. This is generally consistent with observation of the dust gridding phenomenon where the dust particles acquire the spatial orientation of the wire mesh that is at the top electrode, but the particles themselves are suspended as much as 4 cm below the top electrode. In both cases, it could have been expected that the collisions with the neutral atoms would have prevented the formation of these extended structures. A continuing subject for study in both systems is the microprocesses that lead to the long extent along the magnetic field line.

The second observation is that both phenomena appear to be dependent upon ion magnetization; i.e. ion-neutral collisionality. This paper has reported in figure 3 that, as a function

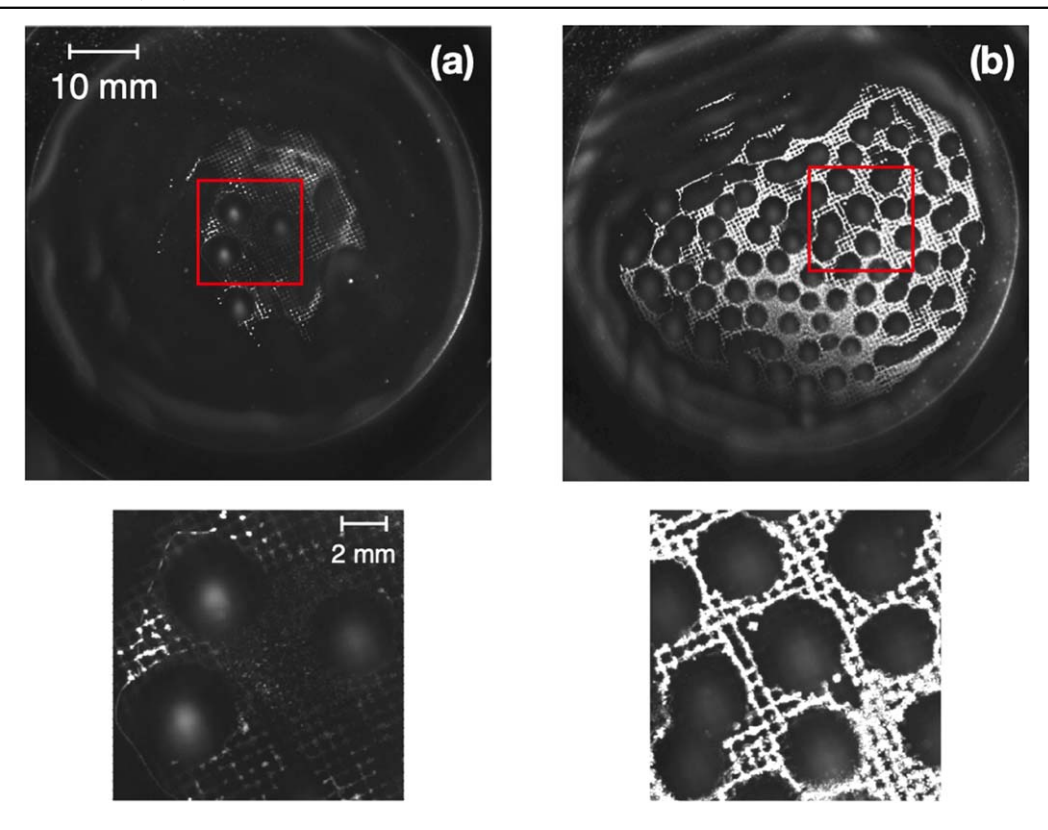


Figure 8. Images showing the coexistence of the filaments with the dust grid structures. The images are the maximum intensity over a sum of 50 individual images for each case. (a) B = 1.5 T, P = 4.0 Pa, rf power = 2.5 W (b) B = 2.0 T, P = 8.0 Pa, rf power = 2.5 W. Below each image is a close-up of the regions that are highlighted in the red boxes. These close-up images provide a clearer view of the interaction between the filaments and the dust particles.

of the increasing neutral pressure, the filaments dissipate as the collisions with neutral atoms begin to dominate the properties of the plasma. As in shown Thomas et al [37], this is the same process that occurs for the dust gridding; increasing the neutral pressure leads to the detrapping of the dust grains. While this qualitative similarity may be important, there are, again, unanswered questions. Between $B = 0.75 \,\mathrm{T}$ and $B = 2 \,\mathrm{T}$, the ion gyroradius for room temperature ions decreases from \sim 0.22 to 0.08 mm. Since this is considerably smaller than the collision mean free path (\sim 1–3 mm) and, at the higher magnetic fields, smaller than the measured size of either the grid wires $(\sim 0.25 \text{ mm})$ or the filaments $(\sim 1 \text{ mm})$, the most pressing question is: what are the physical processes that are occurring between the electrons and ions so that, as the ion magnetization increases, the dust particles can become trapped in a grid pattern and filaments can be formed?

5. Discussion

To address these fundamental questions about the underlying processes that lead to plasma filamentation and gridding, we consider the results of recent numerical simulations. In a recently published paper by Menati, Thomas, and Kushner [40], a two-dimensional simulation of a strongly magnetized, rf generated plasma system motivated by the MDPX configuration was performed using the hybrid plasma equipment

model (HPEM) code [43]. In this simulation, filaments are self-consistently generated in a capacitively-coupled discharge configuration in which one electrode was a powered conductor and the other electrode was covered by a dielectric plate. It is shown that charge accumulation on the dielectric was responsible for creating a perturbation that triggered the formation of filaments along the magnetic field lines. While this model was not directly a simulation of the MDPX device, it does help to provide some insights into the processes that could lead to the formation of a filament.

A parallel simulation effort by Menati is focused on a three-dimensional fluid model that is more closely based on the MDPX configuration. In these simulations, the formation of the filamentary structures is triggered by introducing a 2 mm diameter perturbation to the electron and ion density parallel to the magnetic field. Once this perturbation is made, the system is allowed to evolve self-consistently. A full description of the simulation is beyond the scope of this paper but will be the subject of a forthcoming manuscript; some preliminary results of these simulations are presented here.

Figure 9 shows plots of the evolution of the electron plasma density in a fluid simulation at $B=1\,\mathrm{T}$ at a pressure of $P=10\,\mathrm{Pa}$, starting with three, 2 mm diameter columns that have an electron and ion density of $n_e=n_i\sim 10^{15}\,\mathrm{m}^{-3}$, a factor of ten above the background density of $n_e\sim 10^{14}\,\mathrm{m}^{-3}$. The simulation assumes a constant electron temperature of $T_e=2\,\mathrm{eV}$, but does not include an explicit power balance, so a

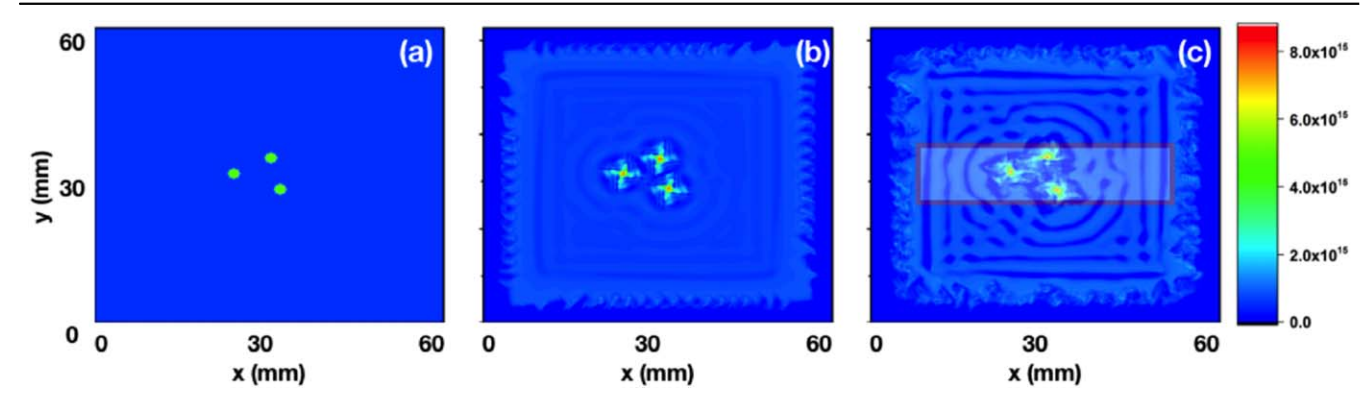


Figure 9. Results of a three-dimensional fluid simulation of plasma filaments. Three, 2 mm diameter filaments are introduced into a uniform plasma with an electron density ten times larger than the background plasma density. Three times are shown in the simulation (a) $t = 0 \mu s$, (b) $t = 15 \mu s$, and (c) $t = 30 \mu s$. The simulation results show the formation of ring-like structures around the main perturbations that appear in the plasma with the main filament columns remaining at the center of the simulation volume. The boxed region highlighted in figure 7(c) is used to compute the average 'intensity' profile that is used in figure 10.

full evaluation of the effect of scaling RF power is not yet possible at this time. The choice of three initial filaments shown here was made to reflect the central region of the rings as shown in figures 7(a)–(d) and the choice of a ten times higher density was to allow a reduced computational time needed to form the rings. It is noted that use of a single, initial column with a lower initial density would also produce the same qualitative structure that is shown in figure 9 and our analysis of the simulation results would remain unchanged.

Here, the profiles of electron density are used as a proxy for the location of the filaments since, in the experiment, it is believed to be the light emission from excited ions and neutrals (via electron impact) that allows us to identify the filaments. Similar to the two-dimensional HPEM simulations, the three-dimensional fluid simulations show the fast evolution of the filamentary structures [40]. It is shown that over the $\Delta t = 30~\mu s$ time span shown in the simulations, there is the formation of a ring-like structure. This ring forms around the central perturbations and extends to the boundaries of the simulation.

One key difference between the simulations and the experiments is the use of a close square boundary in the simulation as compared to the circular geometry of the experiment. Additionally, neither simulation approach has been able to run long enough to reach the millisecond to second timescales of the experiments—which will remain a long-term challenge to making direct comparisons between the experiments and the simulations.

Additionally, figure 10 that shows a qualitative comparison of the density (light intensity) fluctuations relative to the center of each plot. The model data is compared against the 5 W data set shown in figure 7(a). The model data shows a spatial 'ring' structure that has a scale size that is comparable to what is seen in the experiment. We believe this is comparison reasonable since the simulation is initiated with a density column whose initial spatial size is set at 2 mm, similar to what is observed in the experiment.

In spite of these limitations, the simulations do provide us with useful insights. Perhaps the most important result of both

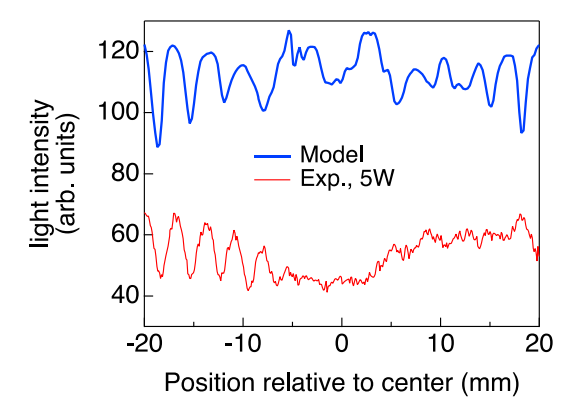


Figure 10. Qualitative comparison of the density (intensity) profiles relative to the center of the analysis region for the simulation results shown in figure 9(c) and the experimental data shown in figure 7(a).

simulations is the need to establish a perturbation in the plasma in order for the filamentary structure to form. Whether this occurs due to a charge buildup or due to the direct introduction of a perturbation, a vertical column of increased plasma density forming along a magnetic field line appears to qualitatively lead to the formation of a structure that has properties similar to the filaments observed in the plasma. This observation may also provide some insights for the dust gridding. If the wire mesh can be treated as a perturbing surface in the plasma, then it could be the source of a vertical structure that extends along the magnetic field line into the plasma. A common physical mechanism that gives rise to both phenomena could provide additional support for their coexistence in the plasma.

In summary, this paper discusses two phenomena that illustrate pattern formation in strongly magnetized plasmas and magnetized dusty plasmas: plasma filamentation and dust gridding. For both processes, the experimental measurements show that increasing ion magnetization (i.e. decreasing the neutral pressure) is correlated with the formation of both the dust gridding and individual filamentary structures in the plasma. In experiments that investigated the role of rf power

on the filaments, it was found that increasing the rf power may lead to a transition from discreet filaments, to larger filament rings and eventually to fluctuating, small-scale structures. However, improved imaging tools may be needed in order to fully resolve this transition. Finally, recent simulations of filaments have shown that there is the formation of extended vertical, filamentary structures in the plasma that are qualitatively similar to those that appear in the experiment, although the simulation results had restricted time and space scales as compared to the experimental conditions.

Acknowledgments

The MDPX device was designed and built with support of the U. S. National Science Foundation (NSF) through the Major Research Instrumentation program (Grant Number PHY-1126067). Additional funding for construction was provided by Auburn University. Support for current experiments is provided by: the NSF EPSCoR program (OIA-1655280) and NSF grants (PHY- 1613102, 1613087 and PHY-1740784). Additional funding is provided by the U. S. Department of Energy Office of Fusion Energy Sciences (SC-0016330) and the US Department of Energy-Plasma Science Facility Program (SC-0019176).

ORCID iDs

E Thomas Jr https://orcid.org/0000-0002-7747-0284

References

- [1] Shukla P K 2001 A survey of dusty plasma physics *Phys. Plasmas* 8 1791–803
- [2] Piel A and Melzer A 2002 Dynamical processes in complex plasmas Plasma Phys. Control. Fusion 44 R1–26
- [3] Luo Q Z, D'Angelo N and Merlino R L 1999 Experimental study of shock formation in a dusty plasma *Phys. Plasmas* 6 3455–8
- [4] Samsonov D, Goree J, Thomas H M and Morfill G E 2000 Mach cone shocks in a two-dimensional Yukawa solid using a complex plasma *Phys. Rev.* E 61 5557–72
- [5] Fortov V E, Petrov O F, Molotkov V I, Poustylnik M Y, Torchinsky V M, Naumkin V N and Khrapak A G 2005 Shock wave formation in a dc glow discharge dusty plasma *Phys. Rev.* E 71 036413
- [6] Heinrich J, Kim S-H and Merlino R L 2009 Laboratory observations of self-excited dust acoustic shocks *Phys. Rev. Lett.* 103 115002
- [7] Vaulina O, Samarian A, Petrov O and James B 2004 Formation of vortex dust structures in inhomogeneous gas-discharge plasmas *Plasma Phys. Rep.* 30 918–36
- [8] Tsai Y-Y and Lin I 2014 Observation of self-excited acoustic vortices in defect-mediated dust acoustic wave turbulence *Phys. Rev.* E 90 013106
- [9] Kaur M, Bose S, Chattopadhyay P K, Sharma D, Ghosh J, Saxena Y C and Thomas E Jr 2015 Generation of multiple toroidal dust vortices by a non-monotonic density gradient in a direct current glow discharge plasma *Phys. Plasmas* 22 093702

- [10] Piel A, Homann A and Melzer A 1999 Laser-excited waves in a plasma crystal *Plasma Phys. Control. Fusion* 41 A453–61
- [11] Piel A, Nosenko V and Goree J 2006 Laser-excited shear waves in solid and liquid two-dimensional dusty plasmas *Phys. Plasmas* 13 042104
- [12] Menzel K O, Arp O and Piel A 2010 Spatial frequency clustering in nonlinear dust-density waves Phys. Rev. Lett. 104 235002
- [13] Merlino R L 2014 25 years of dust acoustic waves J. Plasma Phys. 80 773–86
- [14] Chu J and Lin I 1994 Direct observation of coulomb crystals and liquids in strongly coupled rf dusty plasmas *Phys. Rev.* Lett. 72 4009–12
- [15] Thomas H, Morfill G, Demmel V, Goree J, Feuerbacher B and Möhlmann D 1994 Plasma crystal: coulomb crystallization in a dusty plasma *Phys. Rev. Lett.* 73 652–5
- [16] Thomas H M and Morfill G E 1996 Melting dynamics of a plasma crystal *Nature* 379 806–9
- [17] Couëdel L, Nosenko V, Zhdanov S K, Ivlev A V, Thomas H M and Morfill G E 2009 First direct measurement of optical phonons in 2D plasma crystals *Phys. Rev. Lett.* 103 215001
- [18] Feng Y, Goree J and Liu B 2012 Observation of temperature peaks due to strong viscous heating in a dusty plasma flow *Phys. Rev. Lett.* 109 185002
- [19] Konopka U, Samsonov D, Ivlev A and Goree J 2000 Rigid and differential plasma crystal rotation induced by magnetic fields *Phys. Rev.* E 61 1890–8
- [20] Sato N, Uchida G, Kaneko T, Shimizu S and Iizuka S 2001 Dynamics of fine particles in magnetized plasmas *Phys. Plasmas* 8 1786–90
- [21] Ishihara O, Kamimura T, Hirose K and Sato N 2002 Rotation of a two-dimensional Coulomb cluster in a magnetic field *Phys. Rev.* E 66 046406
- [22] Pilch I, Piel A, Trottenberg T and Koepke M 2007 Dynamics of small dust clouds trapped in a magnetized anodic plasma *Phys. Plasmas* 14 123704
- [23] Schwabe M, Konopka U, Bandyopadhyay P and Morfill G E 2011 Pattern formation in a complex plasma in high magnetic fields *Phys. Rev. Lett.* 106 215004
- [24] Vasiliev M M, D'yachkov L G, Antipov S N, Huijink R, Petrov O F and Fortov V E 2011 Dynamics of dust structures in a dc discharge under action of axial magnetic field EPL 93 15001
- [25] Puttscher M and Melzer A 2014 Dust particles under the influence of crossed electric and magnetic fields in the sheath of an rf discharge *Phys. Plasmas* 21 123704
- [26] Bellan P M 2016 Orbits of magnetized charged particles in parabolic and inverse electrostatic potentials *J. Plasma Phys.* 82 615820101–19
- [27] Tadsen B, Greiner F and Piel A 2018 Probing a dusty magnetized plasma with self-excited dust-density waves *Phys. Rev.* 97 033203
- [28] Thomas E Jr, Merlino R L and Rosenberg M 2012 Magnetized dusty plasmas: the next frontier for complex plasma research Plasma Phys. Control. Fusion 54 124034
- [29] Thomas E Jr, Lynch B, Konopka U, Merlino R L and Rosenberg M 2015 Observations of imposed ordered structures in a dusty plasma at high magnetic field *Phys. Plasmas* 22 030701
- [30] Thomas E Jr, Konopka U, Lynch B, Adams S, LeBlanc S, Merlino R L and Rosenberg M 2015 Quasi-discrete particle motion in an externally imposed, ordered structure in a dusty plasma at high magnetic field *Phys. Plasmas* 22 113708
- [31] Hall T, Thomas E Jr, Avinash K, Merlino R and Rosenberg M 2018 Methods for the characterization of imposed, ordered structures in MDPX *Phys. Plasmas* 25 103702
- [32] Thomas E, Merlino R L and Rosenberg M 2013 Design criteria for the magnetized dusty plasma experiment *IEEE Trans*. *Plasma Sci.* 41 811–5

- [33] Thomas E, DuBois A M, Lynch B, Adams S, Fisher R, Artis D, LeBlanc S, Konopka U, Merlino R L and Rosenberg M 2014 Preliminary characteristics of magnetic field and plasma performance in the magnetized dusty plasma experiment (MDPX) J. Plasma Phys. 80 803–8
- [34] Thomas E, Konopka U, Artis D, Lynch B, LeBlanc S, Adams S, Merlino R L and Rosenberg M 2015 The magnetized dusty plasma experiment (MDPX) J. Plasma Phys. 81 345810206
- [35] Tadsen B, Greiner F and Piel A 2014 Preparation of magnetized nanodusty plasmas in a radio frequency-driven parallel-plate reactor *Phys. Plasmas* 21 103704
- [36] Konopka U, Schwabe M, Knapek C, Kretschmer M and Morfill G E 2005 Complex plasmas in strong magnetic field environments new vistas in dusty plasmas Fourth Int. Conf. on the Physics of Dusty Plasmas vol 799 (AIP Conference Proceedings) pp 181–4
- [37] Thomas E Jr, Konopka U, Merlino R L and Rosenberg M 2016 Initial measurements of two- and three-dimensional ordering, waves, and plasma filamentation in the magnetized dusty plasma experiment *Phys. Plasmas* 23 055701

- [38] Khrapak S 2013 Practical expression for an effective ionneutral collision frequency in flowing plasmas of some noble gases J. Plasma Phys. 79 1123–4
- [39] Thomas E, LeBlanc S, Hall T, Konopka U, Merlino R L and Rosenberg M 2018 Studies of the modification of Langmuir probe traces in strongly magnetized plasmas using the Magnetized Dusty Plasma Experiment (MDPX) device' 2018 USNC-National Radio Science Meeting, Presentation H5–3 (http://ursi.org/proceedings/MC-USA/USNC-NRSM2018/program/Session_H5.htm)
- [40] Menati M, Thomas E and Kushner M J 2019 Filamentation of capacitively coupled plasmas in large magnetic fields *Phys. Plasmas* 26 063515
- [41] Schneider C A, Rasband W S and Eliceiri K W 2012 NIH image to imageJ: 25 years of image analysis *Nat. Methods* **9** 671–6
- [42] Thomas E Jr 2017 Modeling of particle transport in the magnetized dusty plasma experiment *Japan. J. Plasma Fusion Res.* **93** 586–95
- [43] Kushner M J 2009 Hybrid modelling of low temperature plasmas for fundamental investigations and equipment design J. Phys. D: Appl. Phys. 42 194013